20th International Conference on Renewable Energies and Power Quality (ICREPQ'22)
Vigo (Spain), 27th to 29th July 2022
Renewable Energy and Power Quality Journal (RE&PQJ)
ISSN 2172-038 X, Volume No.20, September 2022

EMI Worsening in a SMPS with Non-linear Inductor

Daniele Scirè[1], Giuseppe Lullo[1], Gianpaolo Vitale[2]

[1] Department of Engineering, University of Palermo, 90128 Palermo, Italy {daniele.scire, giuseppe.lullo (at) unipa.it}

[2] ICAR, Institute for high performance computing and networking, National Research Council (CNR), Via Ugo La Malfa, 153, 90146 Palermo {gianpaolo.vitale (at) icar.cnr.it}

Abstract. This paper is focused on the input current in a Switched Mode Power Supply (SMPS) in which the power inductor is exploited up to the saturation showing a non-linear behaviour. The input current exhibits a distortion due to the non-linearity. The electromagnetic interference (EMI) caused by the ripple at switching frequency, superimposed to the DC value of the input current, requires a suitable design of the input differential mode (DM) filter. The input current is analyzed both in the time and frequency domain for different operating conditions, and it is compared to a SMPS equipped with a traditional linear inductor.

Key words. electromagnetic interference (EMI) filter, Switched Mode Power Supply, power density, nonlinear magnetics, saturable core, inductor.

1. Introduction

Optimizing the power density in Switched Mode Power Supplies (SMPSs) leads the designers to look for new solutions. Among these, the extension of the operating current of power inductors up to saturation (intended as the limit in which the value of the inductance is reduced to one half of the rated value) represents a promising perspective. Indeed, in this case, the size of the power inductor, named non-linear inductor since the inductance curve is non-linear, can be reduced [1], [2]. On the other hand, some additional issues must be considered; among them, the inductance lessening increasing the current must be taken into account [3]–[8]. Concerning the core material, ferrite show low losses in a wide frequency range and high specific resistivity; for this reason, they are mostly adopted in power electronics applications [9].

On the other hand, ferrite exhibits an abrupt fall of the inductance approaching saturation, accentuating the increase of the current and the temperature outside the linear zone [3], [10], [11]. Consequently, the current flowing through the power inductor differs from the classical triangular waveform and exhibits a higher peak value approaching saturation. Besides, other phenomena to be considered are an increase of the losses, and the dependence of inductance on the temperature [12]–[14]. Finally, the employment of non-linear inductors increases the electromagnetic interference (EMI) [15], requiring the design of the input filter, according to the spectrum harmonic content [16], with a lower cut-off frequency [17]. Since the input filter affects the power density of the SMPS, it must be taken into consideration into the design phase [18], [19].

This paper aims to show the effects on the EMI caused by the current flowing through the power inductor embedded in the SMPS. Although a non-linear inductor allows saving size and cost, the EMI worsening requires different parameters for the filter design.

The use of a linear inductor is compared with an inductor of the same rated value exploited up to the saturation, operated in the same SMPS. Results, in terms of the input current of the SMPS, are given both in time and frequency domain showing the worsening of EMI when the non-linear inductor is adopted.

The paper is organized as follows: section 2 gives theoretical background on the effects of using a non-linear inductor on EMI, section 3 describes the experimental test rig, and sections 4 and 5 are dedicated to the experimental results in time and frequency domains, respectively; section 6 contains a discussion about results, and finally conclusions are given in section 7.

2. Theoretical background

In a Boost converter with a linear inductor operated in continuous conduction mode (CCM), the calculation of the current variation and its peak value is straightforward. Indeed, considering that during T_{ON} the inductor experiences a constant voltage V_L and its inductance remains constant, the current increases linearly with time and the current variation is retrieved by the inductor's equation:

$$\Delta i_L = i_{L\_max} - i_{L\_min} = \frac{1}{L}\int_0^{T_{ON}} V_L dt = \frac{V_L T_{ON}}{L} \quad (1)$$

The maximum current $i_{L,max}$ is obtained by:

$$i_{L\_max} = i_{L\_min} + \Delta i_L = \overline{i_L} + \frac{\Delta i_L}{2} \quad (2)$$

where the mean current in the inductor is imposed by the load:

$$\overline{i_L} = i_{load}\left(1 - \frac{T_{ON}}{T}\right) \quad (3)$$

Differently, exploiting the saturation, the inductance that is lowered increasing the current peak; hence, it does not exhibit a triangular waveform. It can be explained based on the constitutive equation of the inductance: $V_L = L(\frac{di}{dt})$ where a decrease of the inductance corresponds to an increase of the derivative with the same voltage applied to the inductor as in a boost converter. The two different waveforms of the current corresponding to the linear and non-linear inductor are sketched in figure 1. It can be noted that, compared to the triangular waveform given by the linear inductor, the minimum value is lower, and the maximum value is much higher for the non-linear inductor. The mean value does not vary (neglecting losses) since it depends on the load. Consequently, the current variation in the non-linear case $\Delta i_{L,nl}$ is expected to be higher than the linear case Δi_L. The increase of the maximum value of the current stresses the power switch and the inductor because Joule losses are increased [13], [20–23].

Since the inductance is not constant, eq. (1) cannot be used to calculate $\Delta i_{L,nl}$; instead, the relationship between the inductor voltage and the flux Φ has to be considered:

$$v_L(t) = \frac{\partial}{\partial t}\Phi(i,T) \tag{4}$$

Then, considering that during the T_{ON} time the temperature is constant as well as the voltage applied to the inductor, eq. (4) gives:

$$V_L = \frac{\partial}{\partial i}\Phi(i,T)\frac{d}{dt}i(t) = L(i,T)\frac{d}{dt}i(t) \tag{5}$$

Eq. (5) can be solved numerically once the inductor is characterized by obtaining the curve shown in figure 1.

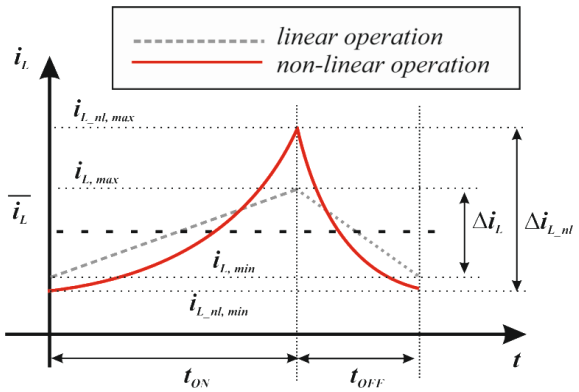

Fig. 1. Current waveforms in linear and non-linear operation of the power inductor

As far as EMI is concerned, a different spectrum is expected with a higher value of the fundamental component and more harmonics with increased amplitude. Besides, the increase of the RMS value of the current implies the need to design the input EMI filter with a lower cut-off frequency [17]. The approach described in [17], and here summarized, allows calculating the cut-off frequency of the input differential mode (DM) filter considering the RMS value of the noise current measured at the terminals of a LIne Stabilization Network (LISN).

$$U_{LISN} = 50\ \Omega \cdot I_{noise\_rms} \tag{6}$$

Where $\boldsymbol{I_{noise\_rms}}$ is the noise current to be filtered and 50Ω is the LISN impedance. The voltage peak at the design frequency of the DM filter f_D is calculated based on the LISN estimated voltage.

$$U_{est}(f_D)[dB\mu V] = 20\ Log\left(\frac{U_{LISN}}{m^a}\frac{1}{\mu V}\right) \tag{7}$$

Where m is a correction factor given by rounding up the ratio between 150 kHz and the switching frequency of the converter and the exponent a is equal to 2 for a triangular waveform. Once the required attenuation is estimated to comply with the required Standard, the LC filter attenuation is:

$$Att_{LC}(f_D) = (2\pi \cdot f_D)^{2\cdot nf} \cdot (2L)^{nf} \cdot C_{x1}^{nf} \geq A_{req\_att}(f_D) \tag{8}$$

It can be noted that by increasing the RMS value of the noise current, as in the case of non-linear inductor, the estimated voltage at the LISN terminals will be increased as well, demanding a higher attenuation by the DM filter to be satisfied with a lower cut-off frequency. The proposed analysis aims to analyze the increase of the RMS value of the current through the power inductor operated up to saturation, together with the spectrum, since it directly influences the DC EMI input filter design.

3. The experimental test rig

A boost converter has been chosen as SMPS. It adopts a MOSFET FDP12N60NZ as power switch and a STTH806 rectifier as free-wheel diode. It is supplied by Vs=12 V with a constant duty cycle of 50% . The electric scheme is shown in figure 2.

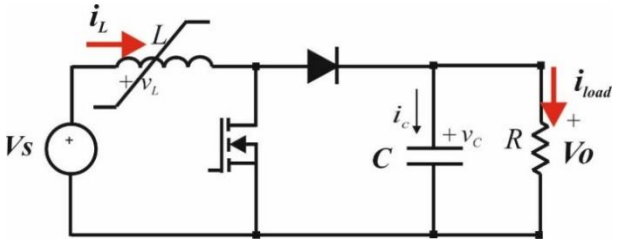

Fig. 2. Schematics of the boost converter

This converter has been equipped for the tests with two SMD ferrite core inductors of 100 µH rated value made by Coilcraft. They are the models DO5040H-104 and DO5010H-104 respectively [24], [25]. The manufacturer assures for the model DO5040H-104 a 10% linear threshold current (intended as the DC current at which the inductance drops 10% from its rated value) of 5.6 A. For the model DO5010H-104, the linear threshold current equals 3 A. However, we extend the use of this inductor up to the saturation current, defined as the current where the differential inductance is reduced to half of its maximum value. It corresponds to a current of about 4 A.

To show the saturation effect, the inductor DO5010H-104 has been characterized by a dedicated measurement

system from which the curve of inductance vs. current has been retrieved [26], [27]. Its characteristic curve is given in figure 3. It can be noted that the inductor DO5010H-104 shows an inductance that decreases with the current; at about 4 A its value is halved respect to the rated one, which corresponds to the saturation limit. It should be remarked that the saturation limit differs from the deep saturation (also known as hard saturation) where the flux density is almost constant. It should be remarked that the deep saturation is of interest for power electronics applications. In the same figure the value of the inductance DO5040H-104 is represented as a horizontal line. With this choice, up to 4 A, the inductor DO5040H-104 will be operated with constant inductance (i.e., in its linear zone); differently, the inductor DO5010H-104 operated up to 4 A will show a saturation effect. In both cases, the threshold current has been set to 4 A. A picture of the two inductors is given in figure 4 where the different sizes can be appreciated. Indeed, the inductor DO5040H-104 (left) employs a bigger core and more copper. The main parameters of the two inductors are summarized in Table I; the size is evaluated considering the maximum footprint; the cost corresponds to the purchase of a single sample net of VAT. It can be noted that the non-linear inductor allows saving of cost, size, and weight.

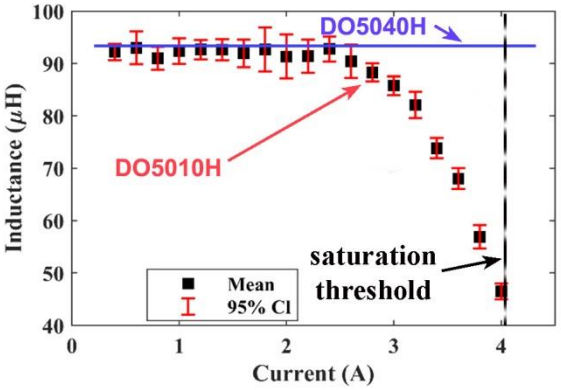

Fig. 3. Inductance vs. current curves for the two inductors under study

Fig. 4. The two inductors under study; DO5040H-104 (left) and DO5010H-104 (right).

Table I. - Parameter Comparison of the two inductors adopted for the test

Inductor	Weight [g]	Size [mm^3]	Cost [€]
DO5040H	5.9	4039	2.95
DO5010H	3.7	1954	2.31

It should be remarked that the DC output voltage of the SMPS always shows the same value, equal to 24V, whatever the adopted inductor during tests. It means that using the non-linear inductor does not influence the DC behavior; differently, the voltage ripple will be different according to the following tests.

4. Time-domain Results

The results presented in this section are focused on the current flowing through the power inductor, it is the same current flowing through the input terminals. Comparing the linear and the non-linear inductor behaviour, it is shown how in this last case, the current waveform depends on the operating point and the switching frequency.

A. Linear inductor time-domain behaviour

The following two tests aim to show that with an inductor operated in the linear zone (meaning with constant inductance), the current waveform remains triangular, whatever the operating conditions.

- Test case #1

In test 1 the inductor DO5040H-104 is subjected to a mean current of about 3 A so that imposing a ripple ΔI_L=1.16 A the maximum current reaches 3.61 A achieved with a switching frequency of 50 kHz. Figure 5a shows the corresponding current variation (blue line) around the DC value (yellow dot) on the inductance curve. The corresponding current waveform is given in figure 5b.

It can be noted that the waveform shows a triangular shape. This shape does not vary if the mean current is decreased up to the CCM limit (corresponding to an increase in the resistance load).

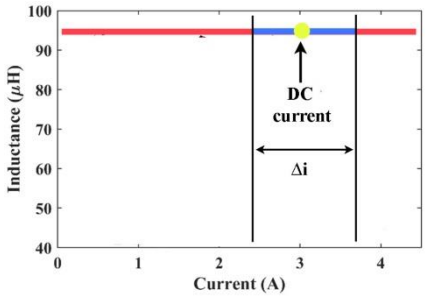

Fig. 5a. DC value of the current and its variation on the inductance characteristic for the test case #1

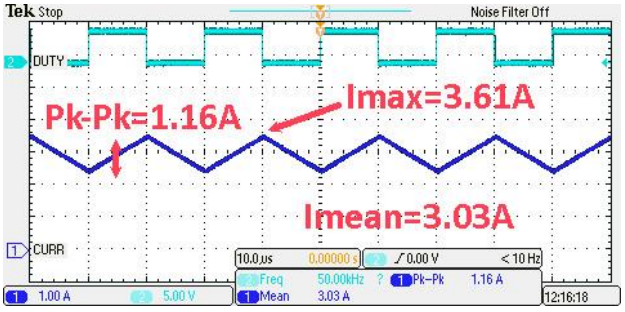

Fig. 5b. current waveforms and main parameters for the test case #1

- Test case #2

Test #2 is conceived to span all the operating region of the inductor by reducing the switching frequency to 16 kHz; the mean current is about 2 A so that imposing a ripple ΔI_L=3.5 A, the maximum current reaches almost 4 A. Also, in this case, the current waveform remains triangular even with such a higher ripple. Figure 6a shows the corresponding current variation (blue line) around the DC value (yellow dot) on the inductance curve. The corresponding current waveform is given in figure 6b.

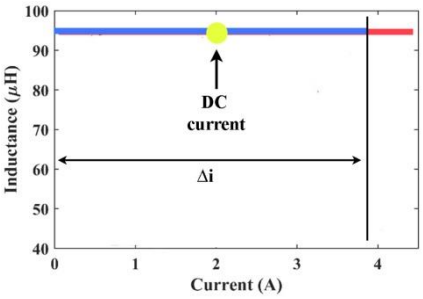

Fig. 6a. DC value of the current and its variation on the inductance characteristic for the test case #2

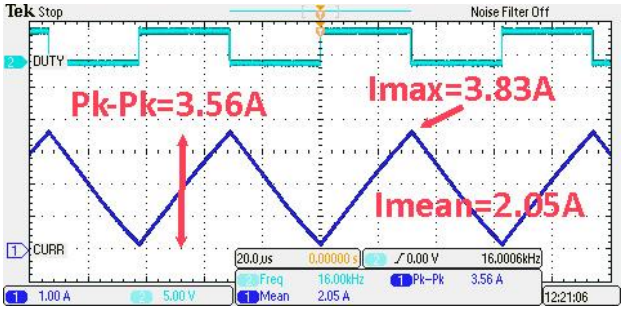

Fig. 6b. current waveforms and main parameters for the test case #2

B. Non-Linear inductor time-domain behaviour

These tests show the effects of exploiting saturation. The inductor DO5010H-104 is used. Concerning the current through the inductor, it depends on the mean current and the ripple. Approaching saturation, the peak increases, and the shape differs from the triangular one.

- Test case #3

This test is performed by imposing a peak-to-peak ripple of 1 A with operation at the threshold between DCM and CCM (corresponding to a minimum value of the current equal to zero). This ripple is obtained by a switching frequency of 50 kHz and duty cycle 50%; these conditions are maintained in the tests #4 and #5 whereas the load is changed to vary the DC current. The waveform of the current is triangular since the linear part of the inductor is exploited. Figure 7a shows the corresponding current variation (blue line) around the DC value (yellow dot) on the inductance curve. It can be noted that, since the inductance remains constant, the behaviour is equal to the corresponding linear inductor. The corresponding current waveform is given in figure 7b.

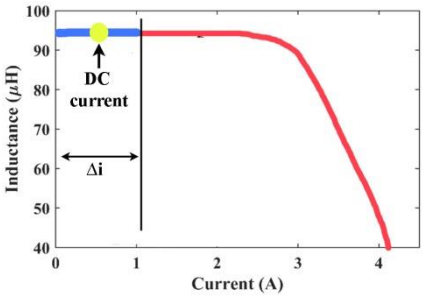

Fig. 7a. DC value of the current and its variation on the inductance characteristic for the test case #3: the current variation affects the linear area of the inductor where its inductance is constant

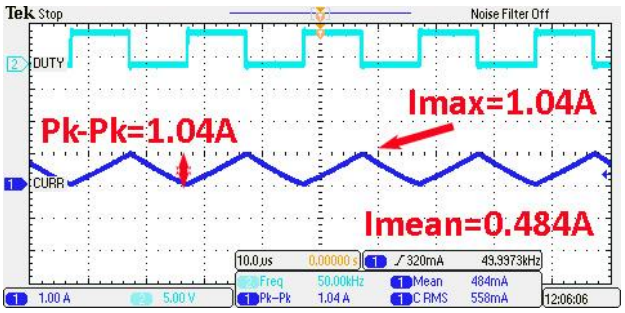

Fig. 7b. Current waveforms and main parameters for the test case #3

- Test case #4

In this test the load resistance value is reduced so that the DC current through the inductor is increased up to 1.94 A. The current ripple slightly increases, and the triangular shape is almost maintained; this small variation is noticed since only the initial part of the characteristic, where the inductance starts decreasing, is exploited.

Figure 8a shows the corresponding current variation (blue line) around the DC value (yellow dot) on the inductance curve. It can be noted that a slight decrease of the inductance is caused by the current. The corresponding current waveform is given in figure 7b.

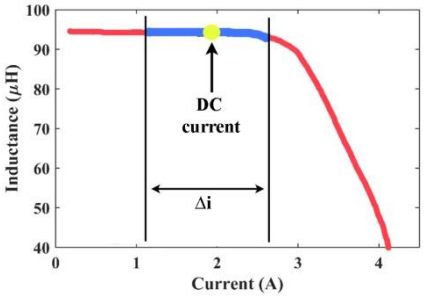

Fig. 8a. DC value of the current and its variation on the inductance characteristic for the test case #4: the current variation lies mostly on a straight line but affects a small part with decreasing inductance

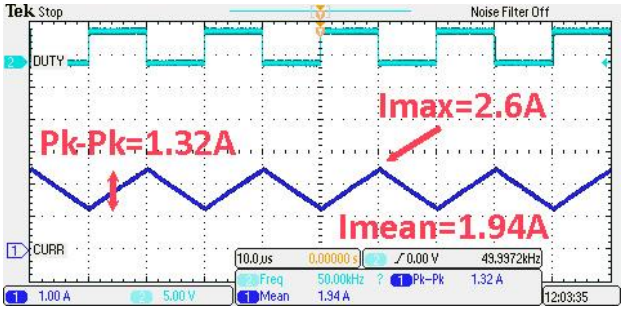

Fig. 8b. Current waveforms and main parameters for the test case #4: an increase of the current ripple compared to the previous test is noticed

- Test case #5

By further reducing the load resistance value, the DC current through the inductor is raised up to 3 A, the non-linear effect is more evident in this test case. The peak-to-peak-value is increased up to 1.88 A and a pronounced peak is visible. Figure 9a shows the corresponding current variation (blue line) around the DC value (yellow dot) on the inductance curve. The DC point lies on the non-linear zone and the decreasing of the inductance for current near the saturation produces a peak. The corresponding current waveform is given in figure 9b. In this case each value of the current corresponds to a different inductance.

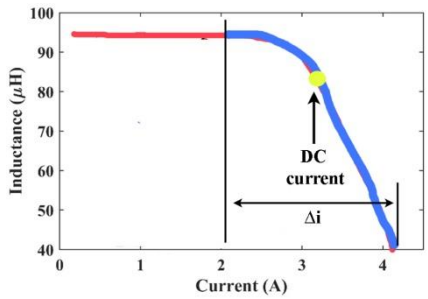

Fig. 9a. DC value of the current and its variation on the inductance characteristic for the test case #5: the current variation interests a part where inductance decreases with the current.

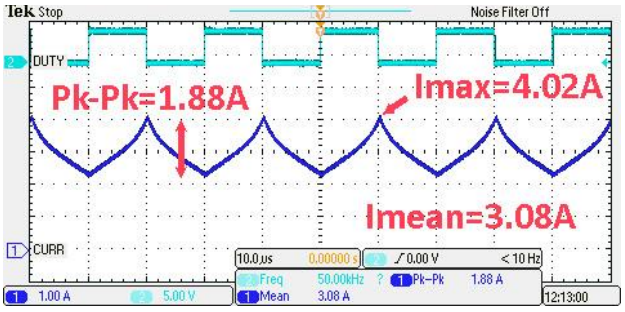

Fig. 9b. current waveforms and main parameters for the test case #5: the current is distorted the current ripple is further increased compared to the previous test

- Test case #6

This test is performed with the same conditions as test #2 (i.e., switching frequency 16 kHz and a mean current of 2 A) but adopting the non-linear inductor. It can be noted that, albeit the load is supplied with the same DC current, a very high ripple is present. The maximum value of the current reaches 4.28 A against the value of 3.83 A obtained in the linear case. Figure 10a shows the corresponding current variation (blue line) around the DC value (yellow dot) on the inductance curve. Here, as in test case #2, by reducing the frequency, all the operating curve is exploited, causing higher current ripple. The corresponding current waveform is given in figure 10b.

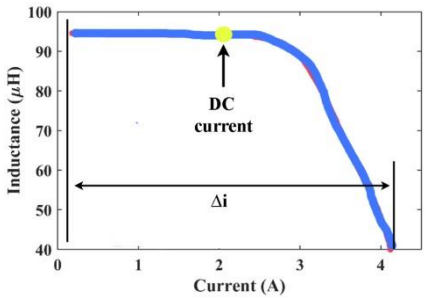

Fig. 10a. DC value of the current and its variation on the inductance characteristic for the test case #6: the current variation interest all the characteristic inductor curve.

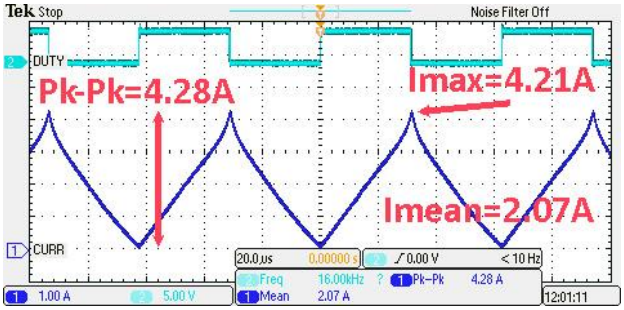

Fig. 10b. current waveforms and main parameters for the test case #6: the current is highly distorted and exhibits a high ripple

The test conditions are summarized in Table II. The grey area corresponds to the linear inductor DO5040H, whereas the white area to the non-linear one DO5010H.

Table II – Test Conditions

Test	Inductor	Fs [kHz]	$\langle I_L \rangle$ [A]	ΔI_L [A]
1	DO5040H	50	3.03	1.16
2		16	2.05	3.56
3	DO5010H	50	0.475	1.02
4		50	1.34	1.32
5		50	3.08	1.88
6		16	2.07	4.28

5. Frequency-domain Results

The Fast Fourier transform (FFT) of the input current is measured in the same test conditions as the previous section. The aim is to highlight the increase of the fundamental frequency corresponding to the switching frequency of the SMPS and the presence of harmonics due to the non-linearity. The harmonics amplitude is given in dBV, it corresponds to the root mean square value of the corresponding harmonic.

A. - Linear inductor frequency-domain behaviour

The inductor DO5040H-104 is operated in linear zone.

- Test case #1

The main harmonic corresponds to the switching frequency set to 50 kHz; the third harmonic is attenuated by about 19 dB. The spectrum is shown in figure 11.

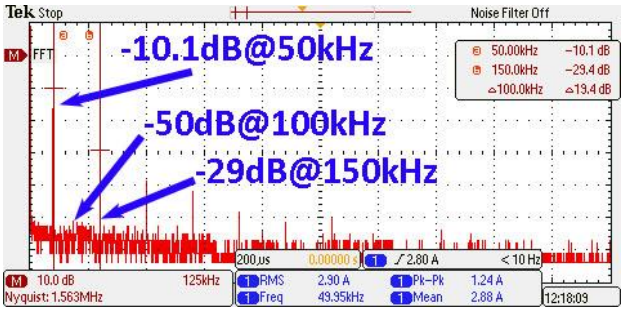

Fig. 11. current spectrum for the test case #1

- Test case #2

The main harmonic corresponds to the switching frequency set to 16 kHz; its amplitude is increased compared to the previous test since the frequency has been lowered; it allows spanning a wider value of inductor characteristics. The third harmonic is attenuated by about 19 dB. The spectrum is shown in figure 12.

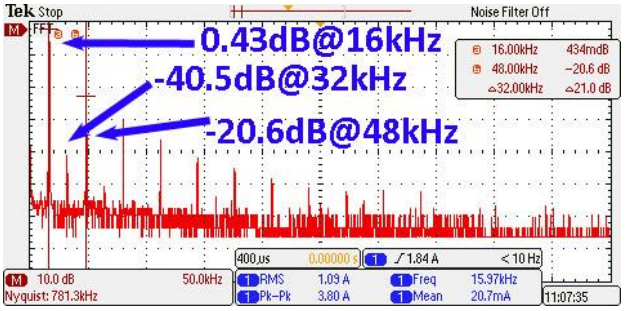

Fig. 12. Current spectrum for the test case #2

B. – Non-linear inductor frequency-domain behaviour

The inductor DO5010H-104 in test #3 is operated starting from a small DC current (corresponding to the linear zone at the threshold of CCM). Then it is increased in test #4 and in test #5 so that the operating range interests the saturation.

- Test case #3

The exploitation of the linear zone implies a fundamental harmonic corresponding to the switching frequency. The third harmonic is reduced by about 19 dB. The spectrum is shown in figure 13.

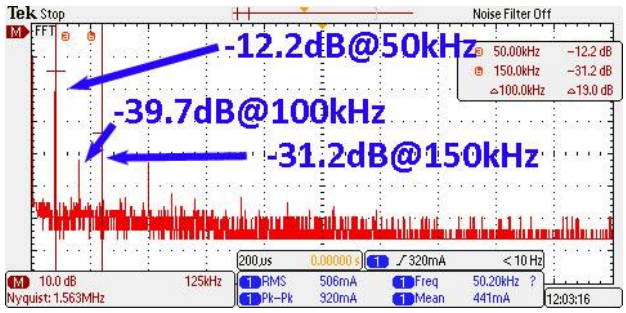

Fig. 13. Current spectrum for the test case #3

- Test case #4

The increase of the DC current, allows reaching the beginning of inductance drop; as a consequence, the fundamental harmonic amplitude is increased. The spectrum is shown in figure 14. Compared to the previous test, the fundamental harmonic is increased by about 3dB; the reduction of the third harmonic compared to the fundamental remains equal to 19dB.

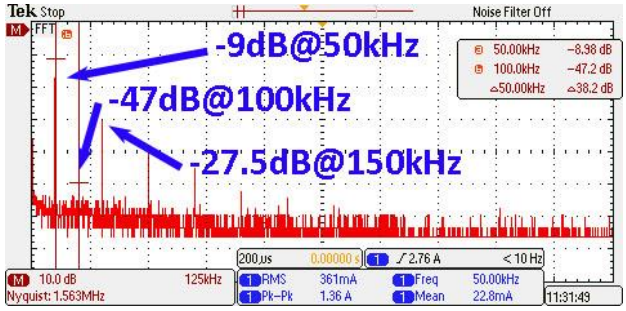

Fig. 14. Current spectrum for the test case #4

- Test case #5

The further increase of the DC current, up to saturation, has raised the fundamental harmonic amplitude and all harmonics. It is relevant that the second harmonic equals the third one. The spectrum is shown in figure 15.

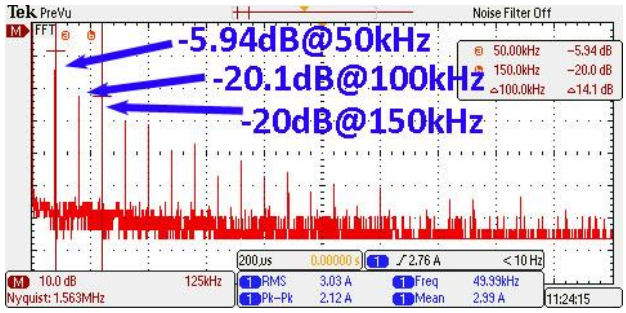

Fig. 15. Current spectrum for the test case #5

- Test case #6

The lowering of the switching frequency to increase the ripple increased the fundamental component. The spectrum is shown in figure 16. Also in this case, the non-linearity of the inductor induces a strong increase of the second harmonic amplitude.

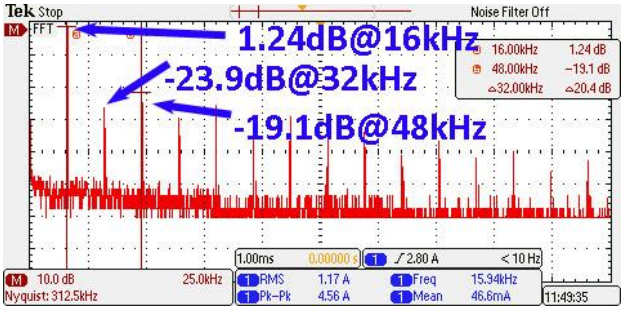

Fig. 16. Current spectrum for the test case #6

The harmonics amplitudes are summarized in table III.

Table III. –Main Harmonics amplitude of the spectrum

Test	Inductor	Fs [kHz]	Amplitude [dB]		
			1st	2nd	3rd
1	DO 5040H	50	-10.1	-50	-29
2		16	0.43	-40.5	-20.6
3	DO 5010H	50	-12.2	-39.7	-31.2
4		50	-9	-47	-27.5
5		50	-5.94	-20.1	-20
6		16	1.24	-23.9	-19.1

C. - Root mean Square analysis

The root mean square of the AC current component plays a crucial role in filter design. As explained in sec. 2, this value is used to choose the cut-off frequency of the input DM filter. The higher the current RMS value, and the lower will be the filter's cut-off frequency, resulting in more expensive. Results are summarized in Table IV. It can be noted that the operation with a high ripple current (obtained by lowering the switching frequency) corresponds to higher RMS. Besides, the saturation exploitation increases the RMS value since the amplitude of either the fundamental or the higher-order harmonics rises.

Table IV. – RMS values of the current

Test	Inductor	$<I_L>$ [A]	RMS (AC) [A]
#1	DO5040H	3.03	0.321
#2		2.05	1.05
#3	DO5010H	0.475	0.254
#4		1.34	0.360
#5		3.08	0.428
#6		2.07	1.18

6. Discussion

The exploitation of a power inductor in a SMPS up to a current in which its inductance is halved, allows using a smaller and cheaper magnetic core. Maintaining the same parameter of the SMPS, so that the output voltage and the supplied power are constant, the EMI related to the use of a traditional linear power inductor has been compared to the EMI generated by a non-linear inductor. Different tests have been proposed varying the DC current.

Test #1 and #2 concern the linear inductor: increasing the DC current, the current shape remains triangular and its spectrum can be easily calculated. The current is triangular also when the ripple spans all the operating range as in test #2.

Test case #3, albeit performed with the DO5010H inductor, does not exploit saturation: as a matter of fact, the DC current is low, corresponding to the CCM threshold: the current waveform and its spectrum still correspond to a linear inductor. The test case #4 showed what happens when the DC current is augmented up to the part of the characteristic in which the inductance starts decreasing: the ripple increases as well as the RMS value of the current and the fundamental harmonic. The saturation exploitation is totally performed in test case #5. It can be noted a further increase of the current ripple and its RMS value; besides, the second harmonic becomes comparable with the third.

Comparing the test case #1 and the test case #5, performed in the same conditions for the two inductors, it is evident the EMI worsening: the first harmonic increases from to -10.1 dBV to -5.94 dBV and the RMS from 0.321 A to 0.428 A. Comparing the test case #2 and the test case #6, performed in the same conditions with a mean current lower compared to the previous test (case #1 and #5) and with a lower switching frequency to increase the ripple up to the saturation for the inductor DO5010H, it can be noted that although the lower switching frequency decreases the switching losses and the higher ripple aids commutation from off to on state occurring at quasi-zero current, the RMS value increases and the amplitude of harmonics.

7. Conclusion

It is well recognized that the exploitation of a power inductor in a SMPS up to the saturation allows reducing the core size and the cost. On the other hand, the shape of the input current differs from the traditional triangular waveforms showing an increase in the peak-to-peak value and a more populated spectrum. This paper shows the effects on the EMI caused by the current flowing through the inductor exploited either in linear and non-linear conditions, evaluating the use of this component up to the saturation. Results, both in the time and frequency domain, show a worsening when the non-linear inductor is adopted. Consequently, the input Differential Mode EMI filter needs to be designed with a lower cut-off frequency than the use of a linear inductor. This contribution must be taken into consideration in the power density optimization.

References

[1] N. Lee, J.-Y. Lee, Y.-J. Cheon, S.-K. Han, and G.-W. Moon, "A High-Power-Density Converter With a Continuous Input Current Waveform for Satellite Power Applications," *IEEE Trans. Ind. Electron.*, vol. 67, no. 2, pp. 1024–1035, Feb. 2020, doi: 10.1109/TIE.2019.2898584.

[2] G. Di Capua and N. Femia, "A novel method to predict the real operation of ferrite inductors with moderate saturation in switching power supply applications," *IEEE Trans. Power Electron.*, vol. 31, no. 3, pp. 2456–2464, 2016, doi: 10.1109/TPEL.2015.2438952.

[3] M. S. Perdigão, J. P. F. Trovão, J. M. Alonso, and E. S. Saraiva, "Large-Signal Characterization of Power Inductors in EV Bidirectional DC-DC Converters Focused on Core Size Optimization," *IEEE Trans. Ind. Electron.*, vol. 62, no. 5, pp. 3042–3051, 2015, doi: 10.1109/TIE.2015.2402632.

[4] A. Oliveri, M. Lodi, and M. Storace, "Nonlinear models of power inductors: A survey," *Int. J. Circuit Theory Appl.*, vol. 50, no. 1, pp. 2–34, Jan. 2022, doi: 10.1002/cta.3147.
[5] G. Di Capua, N. Femia, and K. Stoyka, "An improved algorithm for the analysis of partially saturated ferrite inductors in switching power supplies," in *2016 13th International Conference on Synthesis, Modeling, Analysis and Simulation Methods and Applications to Circuit Design (SMACD)*, Jun. 2016, pp. 1–4, doi: 10.1109/SMACD.2016.7520650.
[6] S. Musumeci, L. Solimene, and C. S. Ragusa, "Identification of DC thermal steady-state differential inductance of ferrite power inductors," *Energies*, vol. 14, no. 13, p. 3854, Jun. 2021, doi: 10.3390/en14133854.
[7] A. Oliveri, M. Lodi, and M. Storace, "A Piecewise-Affine Inductance Model for Inductors Working in Nonlinear Region," in *SMACD 2019 - 16th International Conference on Synthesis, Modeling, Analysis and Simulation Methods and Applications to Circuit Design, Proceedings*, 2019, pp. 169–172, doi: 10.1109/SMACD.2019.8795270.
[8] K. Górecki and K. Detka, "Application of Average Electrothermal Models in the SPICE-Aided Analysis of Boost Converters," *IEEE Trans. Ind. Electron.*, vol. 66, no. 4, pp. 2746–2755, 2019, doi: 10.1109/TIE.2018.2847694.
[9] C. W. T. McLyman, *Transformer and Inductor Design Handbook*, 4th ed. Boca Raton, FL, USA: CRC Press, 2017.
[10] V. C. Valchev and A. Van den Bossche, *Inductors and Transformers for Power Electronics*, 1st ed. Boca Raton, FL, USA: CRC Press, 2018.
[11] G. Vitale, G. Lullo, and D. Scire, "Thermal Stability of a DC/DC Converter With Inductor in Partial Saturation," *IEEE Trans. Ind. Electron.*, vol. 68, no. 9, pp. 7985–7995, Sep. 2021, doi: 10.1109/TIE.2020.3014580.
[12] A. Oliveri, G. Di Capua, K. Stoyka, M. Lodi, M. Storace, and N. Femia, "A power-loss-dependent inductance model for ferrite-core power inductors in switch-mode power supplies," *IEEE Trans. Circuits Syst. I Regul. Pap.*, vol. 66, no. 6, pp. 2394–2402, Jun. 2019, doi: 10.1109/TCSI.2018.2889856.
[13] A. Abramovitz and S. S. Ben-Yaakov, "RGSE-Based SPICE Model of Ferrite Core Losses," *IEEE Trans. Power Electron.*, vol. 33, no. 4, pp. 2825–2831, 2018, doi: 10.1109/TPEL.2017.2762759.
[14] F. Bizzarri, M. Lodi, A. Oliveri, A. Brambilla, and M. Storace, "A nonlinear inductance model able to reproduce thermal transient in SMPS simulations," in *Proceedings - IEEE International Symposium on Circuits and Systems*, May 2019, vol. 2019-May, pp. 1–5, doi: 10.1109/ISCAS.2019.8702418.
[15] D. Scirè, G. Lullo, and G. Vitale, "Non-Linear Inductor Contribution to Harmonic Spectrum in Power Converters," *Proc. XXVI Symp. Electromagn. Phenom. Nonlinear Circuits*, 2021.
[16] D. Scire, G. Lullo, and G. Vitale, "EMI Filter Re-Design in a SMPS with Inductor in Saturation," in *2021 IEEE 15th International Conference on Compatibility, Power Electronics and Power Engineering (CPE-POWERENG)*, Jul. 2021, pp. 1–7, doi: 10.1109/CPE-POWERENG50821.2021.9501176.
[17] K. Raggl, T. Nussbaumer, and J. W. Kolar, "Guideline for a simplified differential-mode EMI filter design," *IEEE Trans. Ind. Electron.*, vol. 57, no. 3, pp. 1031–1040, Mar. 2010, doi: 10.1109/TIE.2009.2028293.
[18] M Di Piazza, A. Ragusa, G. Vitale, G. (2009). Design of grid-side electromagnetic interference filters in AC motor drives with motor-side common mode active compensation. *IEEE Transactions on Electromagnetic Compatibility*, *51*(3), 673-682.
[19]G. Giglia, G. Ala, M. Di Piazza, C. Giaconia, M. Luna, G. Vitale, P. Zanchetta, P. (2018). Automatic EMI filter design for power electronic converters oriented to high power density. *Electronics*, *7*(1), 9.
[20] H. Kosai, Z. Turgut, and J. Scofield, "Experimental investigation of DC-bias related core losses in a boost inductor," *IEEE Trans. Magn.*, vol. 49, no. 7, pp. 4168–4171, 2013, doi: 10.1109/TMAG.2013.2242863.
[21] H. Matsumori, T. Shimizu, X. Wang, and F. Blaabjerg, "A practical core loss model for filter inductors of power electronic converters," *IEEE J. Emerg. Sel. Top. Power Electron.*, vol. 6, no. 1, pp. 29–39, 2018, doi: 10.1109/JESTPE.2017.2761127.
[22] S. Nakano, T. Nakazawa, Y. Matsumoto, and E. Otsuki, "Power loss analysis of SMD power inductors," in *Conference Proceedings - IEEE Applied Power Electronics Conference and Exposition - APEC*, 2011, pp. 1687–1691, doi: 10.1109/APEC.2011.5744822.
[23] S. F. Roberto, D. Scire, G. Lullo, and G. Vitale, "Equivalent Circuit Modelling of Ferrite Inductors Losses," in *IEEE 4th International Forum on Research and Technologies for Society and Industry, RTSI 2018 - Proceedings*, Sep. 2018, pp. 1–4, doi: 10.1109/RTSI.2018.8548450.
[24] Coilcraft Inc., "SMT Power Inductors - DO5010H Series." https://www.coilcraft.com/en-us/products/power/unshielded-inductors/ferrite-drum-surface-mount/do/do5010h/ (accessed Sep. 01, 2020).
[25] Coilcraft Inc., "SMT Power Inductors - DO5040H Series." https://www.coilcraft.com/en-us/products/power/unshielded-inductors/ferrite-drum-surface-mount/do/do5040h/ (accessed Jan. 09, 2020).
[26] D. Scirè, G. Vitale, M. Ventimiglia, and G. Lullo, "Non-Linear Inductors Characterization in Real Operating Conditions for Power Density Optimization in SMPS," *Energies*, vol. 14, no. 13, 2021, doi: 10.3390/en14133924.
[27] M. Ventimiglia, D. Scirè, G. Lullo, and G. Vitale, "A Measurement System for Power Inductors in Non-Linear Operating Conditions," in *IEEE 30th International Symposium on Industrial Electronics (ISIE)*, 2021, pp. 1–6.